Supporting Information (SI)

From Remotely-Sensed SIF to Ecosystem Structure, Function, and Service: *Part I - Harnessing Theory*

Table S1. List of symbols and their definitions

a. Leaf-level variables and parameters (varying with canopy depth L)

Symbols (units)	Definition
A_n (μmol CO_2 m^{-2} s^{-1})	Net Photosynthesis
C_c (Pa)	Chloroplastic CO_2 partial pressure
C_i (Pa)	Intercellular CO_2 partial pressure
F_e (μmol photons m^{-2} s^{-1} nm^{-1})#	The Chl*a*F emission irradiance of a single leaf at λ_F
g_m (umol CO2 m^{-2} s^{-1} Pa^{-1})	Mesophyll conductance of CO_2
g_s (umol CO2 m^{-2} s^{-1} Pa^{-1})	Stomatal conductance of CO_2
I (μmol photons m^{-2} s^{-1} nm^{-1})#	The excitation irradiance at λ_I (i.e., the incident solar irradiance illuminating a leaf at canopy depth L)
J_a (μmol electrons m^{-2} s^{-1})	The actual linear electron transport rate (ETR)
J_{max} (μmol electrons m^{-2} s^{-1})	The maximum electron transport rate
J_{max25} (μmol electrons m^{-2} s^{-1})	J_{max} at 25°C
J_p (μmol electrons m^{-2} s^{-1})	The potential electron transport rate
k_{PAR} (unitless)	The extinction coefficient of PAR under Beer's law
k_{λ_F} (unitless)#	The extinction coefficient of Chl*a*F emission under Beer's law
L (m^2 leaf area m^{-2} ground area)	Canopy depth ($L = 0$ and $L = LAI$ at the top and bottom of the canopy respectively)
NPQ (unitless)	non-photochemical quenching of PSII
O (Pa)	The oxygen partial pressure
p (mol m^{-2} leaf area)	The total concentration of light-harvesting photosynthetic pigments associated with both PSII and PSI per unit leaf area
PAR (μmol photons m^{-2} s^{-1})	The photosynthetically active radiation ($PAR = \int_{400}^{700} I(L, \lambda_I) d\lambda_I$)

q_{LII} (unitless)	The fraction of open PSII reaction centers under the lake model
q_{LI} (unitless)	The fraction of open PSI reaction centers under the lake model
q_7 (unitless)	The fraction of the oxidized PSI donor $P700^+$
R_d (μmol CO_2 m^{-2} s^{-1})	Day respiration
$T_l (^oC)$	Leaf temperature
TPU (μmol CO_2 m^{-2} s^{-1})	The triose phosphate utilization rate
V_{cmax} (μmol CO_2 m^{-2} s^{-1})	The maximum carboxylation rate of Rubisco
V_{cmax25} (μmol CO_2 m^{-2} s^{-1})	V_{cmax} at 25°C
β (unitless)#	The relative contribution of pigments associated with PSII to the overall absorption cross section at λ_I ($1-\beta$ denotes that of PSI)
σ (m^2 mol^{-1})#	The overall leaf-level effective absorption cross section of photosynthetic pigment (which has taken into consideration pigment packaging inside the leaf) at λ_I
$\sigma_{\mathbf{\Omega}\uparrow}$ (m^2 mol^{-1})	The effective specific absorption cross section of photosynthetic pigment for excitation radiance Iat the excitation wavelength λ_I incident at the direction of θ_I projected to the direction of $\mathbf{\Omega}\uparrow$
$\sigma_{\mathbf{\Omega}\downarrow}$ (m^2 mol^{-1})	The effective specific absorption cross section of photosynthetic pigment for excitation radiance Iat the excitation wavelength λ_I incident at the direction of θ_I projected to the direction of $\mathbf{\Omega}\downarrow$.
τ (unitless)#	The transmittance of irradiance
τ_f (unitless)#	The partitioning of Chl*a*F emission in the backward direction
ρ (unitless)#	The reflectance of irradiance
ρ_f (unitless)#	The partitioning of Chl*a*F emission in the forward direction
ω (unitless)#	The leaf scattering coefficient ($\omega = \rho + \tau$)
α (unitless) #	The absorptance of irradiance, i.e., the product of p and σ

α_{vis} (unitless)	The broadband absorption efficiency (i.e., α integrated over the PAR spectral range)
α_T (unitless)	non-returned fraction of the glycolate carbon recycled in the photorespiratory cycle
ε_α (unitless)[#]	The self-absorption probability of Chl*a*F emission ($\varepsilon_\alpha + \varepsilon_\downarrow + \varepsilon_\uparrow = 1$)
$\varepsilon_\downarrow$ (unitless)[#]	The downward escape probability of Chl*a*F emission
$\varepsilon_\uparrow$ (unitless)[#]	The upward escape probability of Chl*a*F emission
$\varepsilon_{\Omega\downarrow}$ (unitless)[#]	The directional escape probability (downward direction) of Chl*a*F emission at sun-canopy-sensor geometry $\boldsymbol{\Omega}$
$\varepsilon_{\Omega\uparrow}$ (unitless)[#]	The directional escape probability (upward direction) of Chl*a*F emission at sun-canopy-sensor geometry $\boldsymbol{\Omega}$
Φ_{PSII} (unitless)	The photochemical quantum yield of PSII
Φ_{PSI} (unitless)	The photochemical quantum yield of PSI
Φ_{FII} (unitless)	The quantum yield of PSII Chl*a*F emission
Φ_{FI} (unitless)	The quantum yield of PSI Chl*a*F emission
Γ^* (Pa)	The chloroplastic CO_2 compensation point (a linear function of oxygen concentration, von Caemmerer, 2000)

Note: m^{-2} refers to "per unit leaf area".
[#] highlight variables that are wavelength-dependent (i.e., spectrally-varying).

b. Canopy-level variables

Symbols (units)	**Definition**
F_{eT} (µmol photons m^{-2} ground area s^{-1} nm^{-1})[#]	Total Chl*a*F emission at λ_F
$F_\uparrow$ (µmol photons m^{-2} ground area s^{-1} nm^{-1})[#]	Upward Chl*a*F irradiance at λ_F leaving top-of-canopy (TOC)
$F_\downarrow$ (µmol photons m^{-2} ground area s^{-1} nm^{-1})[#]	Downward Chl*a*F irradiance at λ_F leaving bottom-of-canopy (BOC)
$F_{\Omega\uparrow}$ (µmol photons m^{-2} ground area s^{-1} nm^{-1} sr^{-1})[#]	Directional (sun-canopy-sensor geometry $\boldsymbol{\Omega}\uparrow$) TOC Chl*a*F radiance at λ_F

Symbols (units)	Definition
$F_{\mathbf{\Omega}\downarrow}$ (μmol photons m^{-2} ground area s^{-1} nm^{-1} sr^{-1})#	Directional (sun-canopy-sensor geometry $\mathbf{\Omega}\downarrow$) BOC Chl*a*F radiance at λ_F
f^{esc} (unitless)#	The fluorescence escape probability (i.e., the fraction of F_{eT} escaping from TOC, $f^{esc} = \frac{F_\uparrow}{F_{eT}}$)
$f^{esc}_{\Omega\uparrow}$ (unitless)#	The directional fluorescence escape probability from TOC at (sun-canopy-sensor geometry $\mathbf{\Omega}\uparrow$, $f^{esc}_{\Omega\uparrow} = \frac{F_{\mathbf{\Omega}\uparrow}}{F_{eT}}$)
GPP_T (μmol CO_2 m^{-2} ground area s^{-1})	The total GPP integrated over canopy depth
J_{aT} (μmol m^{-2} ground area s^{-1})	The total actual ETR integrated over canopy depth
LAI (m^2 leaf area m^{-2} ground area)	leaf area index
$\bar{p}$ (mol m^{-2} leaf area)	The mean photosynthetic pigment content of the canopy
$R_{\mathbf{\Omega}\uparrow}$ (unitless)#	The directional reflectance at TOC
$\bar{\beta}$ (unitless)	The canopy-mean broadband β (i.e., integrated over the PAR spectral range 400 to 700nm)
$\bar{\sigma}$ (m^2 leaf area mol^{-1})	The canopy-mean broadband σ (i.e., integrated over the PAR spectral range 400 to 700nm)
$\bar{\Phi}_{PSII}$ (unitless)	The canopy-level photochemical quantum yield of PSII
$\bar{\Phi}_{FII}$ (unitless)	The canopy-level fluorescence quantum yield of PSII (i.e., SIF yield)

Note: m^{-2} refers to either "per unit leaf area" or "per unit ground area", specified in each variable.
highlight variables that are wavelength-dependent.

c. Other variables and parameters

Symbols (units)	Definition
a, b	Empirical parameter for calculating q_{LII} as a function of PAR
a_N, b_N	Empirical parameter for calculating NPQ as a function of PAR

Symbols (units)	Definition
i_0	The canopy directional interceptance (depending on canopy gap fraction)
K_c (Pa)	Michaelis-Menten constant for RuBP carboxylation
K_o (Pa)	Michaelis-Menten constant for RuBP oxygenation
k_D (s^{-1})	The rate constant for internal conversion (constitutive or unregulated heat dissipation)
k_{DF} (unitless)	The ratio of k_D to k_F
k_F (s^{-1})	The rate constant for Chl*a*F emission
k_N (s^{-1})	The rate constant of NPQ for PSII
k_{PMII} (s^{-1})	The maximal (intrinsic) rate constant for photochemical quenching of PSII
k_{PMI} (s^{-1})	The maximal (intrinsic) rate constant of photochemical quenching of PSI
k_7 (s^{-1})	The rate constant of NPQ by $P700^+$
NPQ_0 (unitless)	NPQ at TOC
NPQ_7 (unitless)	The non-photochemical quenching capacity of $P700^+$
PAR_0 (μmol photons m^{-2} s^{-1})	The incoming PAR at TOC
q_{LII0} (unitless)	q_{LII} at TOC
r_s (unitless)[#]	The soil reflectance
S_0	The ground state of chlorophyll
S_1	The first excited state of chlorophyll
s_{II} (unitless)[#]	The spectral shape function (elementary distribution) of Chl*a*F emission of PSII, integrated to unity
s_I (unitless)[#]	The spectral shape function (elementary distribution) of Chl*a*F emission of PSI, integrated to unity
x (unitless)	The fraction of total electron transport of mesophyll and bundle sheath allocated to mesophyll
λ_F (nm)	The Chl*a*F emission wavelength

Symbols (units)	Definition
λ_{Fmax}(nm)	The maximum wavelength of Chl*a*F emission
λ_{Fmin}(nm)	The minimum wavelength of Chl*a*F emission
λ_I(nm)	The excitation light wavelength
λ_{Imin}(nm)	The minimum wavelength of excitation light
Φ_{PSIIm}(unitless)	The maximal photochemical quantum yield of PSII (can be considered as constant ~c. 0.83 across species, Björkman and Demmig, 1987; Johnson et al., 1993)
Φ_{PSIm}(unitless)	The maximal photochemical quantum yield of PSI
θ(unitless)	The curvature parameter (to compute the potential electron transport rate J_p in FvCB)
θ_I	A generic vector representing direction of the excitation radiance
$\boldsymbol{\Omega}\uparrow$	A vector representing the sun-canopy-sensor geometry, including: solar zenith angle (SZA), view zenith angle (VZA) away from TOC towards the sky, and relative azimuth angle (RAA) between the sun and sensor above the canopy
$\boldsymbol{\Omega}\downarrow$	A vector representing the sun-canopy-sensor geometry, including: solar zenith angle (SZA), view zenith angle (VZA) away from BOC towards the ground, and relative azimuth angle (RAA) between the sun and sensor below the canopy
$\varepsilon_{\downarrow 0}$(unitless)[#]	The downward escape probability of Chl*a*F emission for an infinitesimally thin leaf layer at BOC
$\varepsilon_{\uparrow 0}$(unitless)[#]	The upward escape probability of Chl*a*F emission for an infinitesimally thin leaf layer at TOC

Note: m^{-2} refers to "per unit leaf area".
[#] highlight variables that are wavelength-dependent.

Table S2. Summary of existing process-based models that have SIF-simulating capability.

Model	Leaf-level parameterization of Chl*a*F emission		Canopy RTM of SIF	Sun-canopy -sensor geometry	λ_F	Application	Pros	Cons	CE^	Ref
	Leaf RTM	***Biochemical***								
3D (horizontally) heterogeneous canopy - *small scale scenes*										
DART[#]	Fluspect	None	Explicit modeling based on 3D ray-tracing		Full spectra	• Natural landscapes • *DART only*: including urban landscapes	• Suitable for small scale scenes with fine complex composition and structure • *DART only*: Integration with Lidar	• Computationally still too demanding to be applied at large scale (>100m), but more efficient approaches may emerge. • Requiring accurate leaf/canopy structural/functional info as priori input, which are often challenging to obtain • No leaf-level Chl*a*F emission formulation included (except FLiES) • No vertical heterogeneity in vegetation structure • Not yet thoroughly validated with in-situ data		(Gastellu-Etchegorry et al., 2017)
FluorWPS	Fluspect	As a function of PAR[&]								(Zhao et al., 2016)
FluorFLIGHT[#]	Fluspect	None								(Hernández-Clemente et al. 2017)
FLiES	FluoMODLeaf	FvCB + k_N								(Sakai et al., 2020)
FluorRTER	Fluspect	None	Explicit modeling based on SRTE				• Computationally more efficient than the ray-tracing approach • Potential for large-scale applications			(Zeng et al., 2020)
1D (horizontally) homogeneous canopy - *point to landscape scale*										
SCOPE	Fluspect	FvCB + k_N	**• Explicit modeling based on SAIL 4-stream approach** **• Multi-layer canopy (nlayer = 10LAI)[$]**		**Full spectra**	**• Process interpretation** **• Benchmarking for both 3D and global TBMs/LSMs**	**• Computationally more efficient than 3D models** **• Vertical heterogeneity in biochemical and/or biophysical properties**	**• Not suitable for horizontally heterogeneous canopy, e.g., crops with row structure, forests with complex architecture** **• Requiring accurate site-specific leaf/canopy structural/functional info as priori input, which are often challenging to obtain** **• k_N formulation empirical and susceptible to uncertainties in FvCB** **• Impact of biotic stress not represented**		(Van der Tol et al., 2009, 2014; van der Tol et al., 2019; Yang et al., 2017; Yang, Prikaziuk, et al., 2021)

1D (horizontally) homogeneous canopy - *global scale TBMs or LSMs*										
BETHY + SCOPE	Fluspect	FvCB +*	• Multi-layer canopy (nlayer = 60)	• Not explicitly represented • Only output nadir and/or hemispherically-integrated TOC SIF (calibrated to SCOPE ensemble simulations) • *BETHY only*: No info provided • *JSBACH only*: No SIF magnitude, as no wavelength separation	• Single wavelength • A conversion factor calibrated to SCOPE ensemble simulations • *BETHY only*: No info provided on wavelength adjustment	• Global (forward) simulations of SIF for comparison with in-situ and/or satellite SIF retrievals • Data assimilation by ingesting SIF measurements to constrain parameters and/or variables related to GPP simulations	• Computationally most efficient for large-scale simulations • Vertical heterogeneity in biochemical/biophysical properties (for some models)	• Uncertainties in model structure (formulations) and parameters of FvCB, k_N, SIF parameterizations for global PFTs • Simplified SIF leaf-to-canopy RTM formulations • Depend on external simulations of SCOPE for deriving simple conversion factors or parameterizations to account for escape probability at certain viewing angle(s) and specific wavelength		(Koffi et al., 2015)
JSBACH	None	FvCB + q_{LII}	• Multi-layer canopy (nlayer = 3) • Assuming a constant exponential attenuation factor of Chl*a*F emission, calibrated to SCOPE simulations							(Thum et al., 2017)
SiB*	None	FvCB +*	• One "big-leaf" model NOT separating sunlit and shaded portions • Assuming a factor accounting for leaf to canopy scaling calibrated to SCOPE simulations							(Haynes et al., 2020)
ORCHIDEE	None		• A simplified empirical model calibrated to SCOPE ensemble simulations							(Bacour et al., 2019)
BEPS	None		• Two "big-leaf" model accounting for sunlit and shaded portions • Exponential attenuation factor of Chl*a*F emission as a function of LAI and clumping index • Scattering factor of Chl*a*F emission as a function of LAI							(Cui et al., 2020; Qiu et al., 2019)
CLM*	None		• Two "big-leaf" model accounting for sunlit and shaded portions • CLM4: Assuming a factor accounting for leaf to canopy scaling calibrated to SCOPE simulations • CLM5: Separate calculation of canopy-level escape probability for sunlit and shaded portions according to Zeng et al. (2019)	• Empirically represented • Only output nadir and/or hemispherically-integrated TOC SIF						(Lee et al., 2015; Raczka et al., 2019; Li et al., 2022)

[&]Based on Rosema et al. (1998)
[#]RAdiation transfer Model Intercomparison (RAMI) participating model
*Subjective to version differences and/or formulation variants
[^]CE denotes computational efficiency; models are broadly sorted in increasing order of CE, color-coded in a warm (low CE) to cold (high CE) spectrum.
[$]nlayer denotes number of canopy layer

Table S3. Model configuration and parameter setup in SCOPE2.1 for simulations of canopy-level escape probability $f_{\Omega\uparrow}^{esc}$ and reflectance $R_{\Omega\uparrow}$ for a C3 crop canopy in Fig. 3b.

Parameter/Variable	Abbreviation	Values (units)
Canopy structural properties		
Leaf area index	LAI	3
Leaf angle distribution	LIDF	Spherical
Leaf structural and physiological properties		
Chlorophyll a + b content	Cab	40 (μg cm^{-2})
Carotenoid content	Cca	10 (μg cm^{-2})
Dry matter content	Cdm	0.0120 (g cm^{-2})
Water content	Cw	0.0090 (cm)
Brown pigments	Cs	0 (-)
Leaf structure parameter	N	1.5 (-)
Anthocyanin content	Cant	1 (μg cm^{-2})
Protein content	Cp	0 (μg cm^{-2})
Carbon-based constituents	Cbc	0 (μg cm^{-2})
Carboxylation capacity at 25°C	V_{cmax25}	60 (μmol CO_2 m^{-2} s^{-1})
Ball-Berry slope	g_1	8 (-)
Ball-Berry intercept	g_0	0.01 (-)
Illumination and viewing conditions		
Incoming shortwave radiation	Rin	600 (Wm^{-2})
Solar zenith angle	SZA	30
View zenith angle	VZA	0

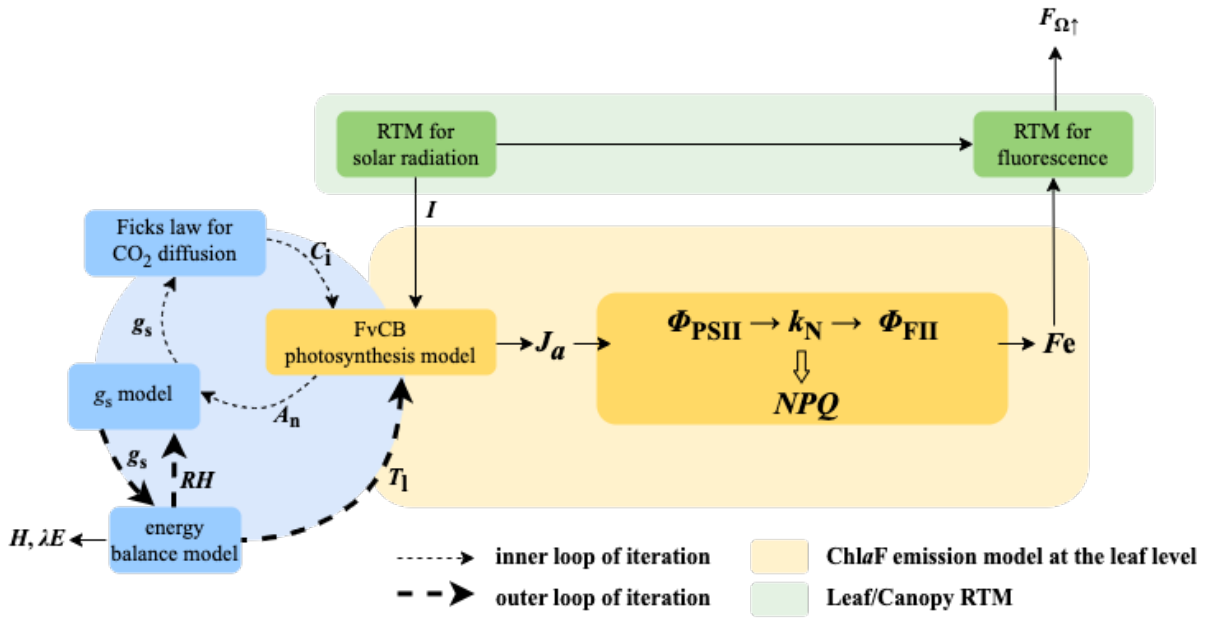

Figure S1. Graphical illustration of the leaf-level calculation of Chl*a*F emission (yellow) and its coupling with energy balance (blue) and leaf/canopy-level radiative transfer modeling (RTM, green). Note we intend to display details disproportionally for different processes. This is because we intend to highlight the FvCB+ k_N strategy (section 2.4 in the main text) in modeling the leaf-level Chl*a*F emission, i.e.,F_e, while paradigms of the nested loop of energy balance and photosynthesis-stomatal conductance model, and leaf/canopy RTM are historically well established (based on laws of physics). The FvCB+ k_N modeling strategy of Chl*a*F emission is built upon the assumption of balanced light and carbon reaction under steady state, an is implemented by SCOPE (van der Tol et al., 2014). Here T_l, H, and λE represent leaf temperature, sensible heat flux, and latent heat flux at the leaf level, respectively. All other symbols are defined in Table S1.

SI – 1. Rationale for considering both PSII and PSI in SIF research

Chl*a*F emissions from both PSII and PSI need to be considered in SIF research for the following reasons:

- In typical PAM fluorometry, it is generally assumed PSI does not contribute to variable Chl*a*F, which is the difference between Chl*a*F yield observed during the application of saturating pulse and that observed after the saturating pulse is switched off and the electrons from the acceptors of PSII have been drained off (Baker, 2008). This assumption stems from a convenient assumption that $P700^+$ quenches the excitation energy non-photochemically as efficiently as its reduced state quenches the excitation photochemically (Kitajima & Butler, 1975). However, this assumption has been increasingly challenged in experiments (Franck et al., 2002; E. E. Pfündel et al., 2013; Schreiber & Klughammer, 2021; Trissl, 1997) and modeling (Lazár, 2013) studies which showed that $P700^+$ does not quench non-photochemically as efficiently as P700 does photochemically.

- Even if we accept the assumption that PSI does not contribute to variable fluorescence, we still cannot assume the Chl*a*F emission of PSI is negligibly small in the context of general SIF applications. PSI uses a bidirectional (symmetrical) mechanism for charge separation whereas PSII employs a monodirectional (asymmetrical) mechanism. As a result, PSI is photochemically more efficient than PSII is (for details, see Caffarri et al., 2014). However, PSI photochemical efficiency is not 100%. Φ_{PSIm} is between 0.94 to 0.98 (Hogewoning et al., 2012) while Φ_{PSIIm} is about 0.83 across species (Björkman & Demmig, 1987; JOHNSON et al., 1993). More importantly, SIF currently can only be observed at specific wavelengths such as Franhaufer lines, O_2A and O_2B bands. We have no guarantee that s_I is much smaller than s_{II} at these specific wavelengths (see Eq 3).
- In typical PAM fluorometry, PSII and PSI are assumed to receive equal allocation of absorbed energy, i.e., $\beta = 0.5$ (Baker, 2008). However, under stress when consumption of ATP increases (see discussions next section), more energy may be allocated to PSI than PSII (i.e., $\beta < 0.5$), potentially increasing PSI fluorescence.

Therefore, PSI cannot be ignored in SIF research until further evidence proves otherwise.

SI – 2. Formulation of directional SIF: $F_{\Omega\uparrow}$ and $F_{\Omega\downarrow}$

$$F_{\mathbf{\Omega}\uparrow}(\lambda_F) = \int_0^{LAI} p(L)\varepsilon_{\mathbf{\Omega}\uparrow}(L,\lambda_F)\int_{\lambda_{Imin}}^{\lambda_F}\{\Phi_{FII}(L)s_{II}(\lambda_F)\beta(L,\lambda_I)+\Phi_{FI}s_I(\lambda_F)[1-\beta(L,\lambda_I)]\}\int\sigma_{\mathbf{\Omega}\uparrow}(\theta_I,L,\lambda_I)I(\theta_I,L,\lambda_I)d\theta_I d\lambda_I dL + \varepsilon_{\mathbf{\Omega}\uparrow}(LAI,\lambda_F)\int r_{s\mathbf{\Omega}\uparrow}(\theta_I,\lambda_F)F_{\theta_I\downarrow}(\lambda_F)d\theta_I \quad \text{(S1)}$$

$$F_{\mathbf{\Omega}\downarrow}(\lambda_F) = \int_0^{LAI} p(L)\varepsilon_{\mathbf{\Omega}\downarrow}(L,\lambda_F)\int_{\lambda_{Imin}}^{\lambda_F}\{\Phi_{FII}(L)s_{II}(\lambda_F)\beta(L,\lambda_I)+\Phi_{FI}s_I(\lambda_F)[1-\beta(L,\lambda_I)]\}\int\sigma_{\mathbf{\Omega}\downarrow}(\theta_I,L,\lambda_I)I(\theta_I,L,\lambda_I)d\theta_I d\lambda_I dL \quad \text{(S2)}$$

Here $F_{\mathbf{\Omega}\uparrow}$ is the radiance of SIF at λ_F traveling in the direction of $\mathbf{\Omega}\uparrow$ away from TOC towards the sky, while $F_{\mathbf{\Omega}\downarrow}$ is the radiance of SIF at λ_F traveling in the direction of $\mathbf{\Omega}\downarrow$ away from BOC towards the soil surface. $\varepsilon_{\mathbf{\Omega}\uparrow}$ and $\varepsilon_{\mathbf{\Omega}\downarrow}$ are the escape probability of a SIF photon emitted at the canopy depth of L into the direction of $\mathbf{\Omega}\uparrow$ and $\mathbf{\Omega}\downarrow$ at TOC and BOC, respectively. $\sigma_{\mathbf{\Omega}\uparrow}$ and $\sigma_{\mathbf{\Omega}\downarrow}$ are the effective specific absorption cross section of photosynthetic pigment for excitation radiance I at the excitation wavelength λ_I incident at the direction of θ_I projected to the direction of $\mathbf{\Omega}\uparrow$ and $\mathbf{\Omega}\downarrow$ respectively. r_s is the spectral reflectance of the soil surface. All directional integrals of θ_I occur on a sphere.

SI – 3. Derivation of Eq 3

Gu et al. (2019) expressed Φ_{FII} as a function of photochemical quenching (i.e., q_{LII}) and NPQ.

$$\Phi_{FII} = \frac{1 - \Phi_{PSIIm}}{(1 + k_{DF})[(1 + NPQ)(1 - \Phi_{PSIIm}) + q_{LII}\Phi_{PSIIm}]} \quad \text{(S3)}$$

Here Φ_{PSIIm} is the maximal photochemical quantum yield of PSII. k_{DF} is the ratio of rate constant for constitutive (unregulated) heat dissipation (k_D) to that for Chl*a*F emission (k_F). Note that Φ_{FII}, q_{LII}, NPQ form a closed equation for PSII, and knowing any two of them is sufficient to resolving the third, assuming Φ_{PSIIm} and k_{DF} are constants.

Here we derive a similar expression for Φ_{FI}. A couple of uncertainties affect the derivation of Φ_{FI}. The first uncertainty is whether PSI undergoes regulated heat dissipation. In the PAM fluorometry literature, the quantity known as NPQ is virtually always implied for PSII because it has been generally believed PSI does not experience non-photochemical quenching in the same way as PSII does. Surprisingly, Ballottari et al., (2014) found that zeaxanthin efficiently quenched fluorescence in PSI particles extracted from an *Arabidopsis thaliana* mutant, implying that a PSII-type NPQ process also occurs in PSI. However, Tian et al., (2017) demonstrated that in wide type *Arabidopsis thaliana*, no zeaxanthin-dependent NPQ existed in PSI. In this review, based on the findings of Tian et al., (2017), we assume that in in vivo, physiologically relevant environmental conditions, no PSII-type NPQ occurs in PSI.

The second uncertainty is related to the capacity of the oxidized electron donor of PSI reaction center ($P700^+$) in dissipating PSI excitation energy into heat. It is accepted that the oxidized electron donor of PSII reaction center ($P680^+$), whose sustained existence results in photodamage (Jegerschoeld et al., 1990), is incapable of non-photochemically dissipating excitation. However, $P700^+$ has been shown to protect PSI by dissipating excess excitation energy into harmless heat (Bukhov & Carpentier, 2003; Sonoike, 2011). A convenient assumption that was first made by Kitajima & Butler (1975) states that $P700^+$ quenches the excitation energy non-photochemically as efficiently as its reduced state quenches the excitation photochemically. A consequence of this assumption is that the variable fluorescence in PAM fluorometry comes only from PSII as the fluorescence yield from PSI does not change between the minimal and maximal fluorescence measurements, which simplifies the interpretation of PAM fluorometry parameters. However, this assumption has been increasingly challenged in experimental (Franck et al., 2002; E. E. Pfündel et al., 2013; Schreiber & Klughammer, 2021; Trissl, 1997) and modeling (Lazár, 2013) studies which showed that $P700^+$ does not quench non-photochemically as efficiently as P700 does photochemically. We accept this contemporary view of $P700^+$ to derive Φ_{FI}.

Based on these considerations, we express Φ_{FI} as the following:

$$\Phi_{FI} = \frac{k_F}{k_F + k_D + q_{LI}k_{PMI} + q_7k_7} \quad \text{(S4)}$$

Here q_{LI} is the fraction of open reaction centers of PSI, q_7 the fraction of the oxidized PSI donor, k_{PMI} the maximal (intrinsic) rate constant of photochemical quenching of PSI, and k_7 the rate constant of NPQ by $P700^+$. Instead of using the cumbersome $P700^+$ as subscript, we have simply used '7' to denote it in q_7 and k_7. We assume that PSII and PSI share the same k_F and k_D values.

To transform Eq S4 into a form analogous to Eq S3, we note that the maximal photochemical quantum yield of PSI (Φ_{PSIm}) is given by

$$\Phi_{PSIm} = \frac{k_{PMI}}{k_F + k_D + k_{PMI}} \tag{S5}$$

From Eq S5,

$$\frac{k_{PMI}}{k_F + k_D} = \frac{\Phi_{PSIm}}{1 - \Phi_{PSIm}} \tag{S6}$$

Analogous to NPQ for PSII, we define the corresponding NPQ of $P700^+$ (NPQ_7) as

$$NPQ_7 = \frac{k_7}{k_F + k_D} \tag{S7}$$

Note that, however, NPQ for PSII dynamically responds to changes in environmental conditions, whereas NPQ_7 is a parameter constant. Thus the NPQ dynamics of PSI is entirely determined by the oxidized fraction of PSI donor q_7. Using Eqs S6-S7, Eq S4 becomes

$$\Phi_{FI} = \frac{1 - \Phi_{PSIm}}{(1 + k_{DF})[(1 + q_7 NPQ_7)(1 - \Phi_{PSIm}) + q_{LI}\Phi_{PSIm}]} \tag{S8}$$

Eq S8 shows that Φ_{FI}, q_7, and q_{LI} are uniquely coupled for PSI and knowing any two of the three is sufficient to resolve the third. Insert Eq S3 and S8 into Eq 2c, we have the complete equation for $F_\uparrow$ in Eq 3 in the main text.

SI – 4. Rationale of parameter constants treatment in Eq 3

For non-stressed plants, Φ_{PSIIm} is constant (~c. 0.83) across species (Björkman & Demmig, 1987; JOHNSON et al., 1993). PSI is photochemically more efficient than PSII (Nelson, 2009), and thus $0.83 < \Phi_{PSIm} < 1$. This means that for a fully relaxed leaf in the dark, the combined quantum yield of fluorescence whose rate constant is k_F(s^{-1}) and internal conversion (constitutive or unregulated heat dissipation) whose rate constant is k_D(s^{-1}) is at most 0.17. k_{DF} (unitless) is the ratio of k_D to k_F. k_D and k_F are physical properties of chlorophyll molecules and their environments. k_D is an intrinsic property of chlorophyll molecules and can be determined by the collision of the excited chlorophyll molecules with solvent molecules whereas k_F is determined by the lifetime of the chlorophyll's first excited singlet state. Because plants have no active mechanisms to regulate k_D and k_F and because the unstressedΦ_{PSIIm}, which equals $k_{PMII}/(k_D + k_F + k_{PMII})$where k_{PMII} is the maximal rate constant for photochemistry of PSII, is constant, it is reasonable to assume $k_F$and k_D and therefore k_{DF} are constant (Gu et al., 2019). However, the precise values of k_F and k_D and thus k_{DF} in vivo are currently unknown. The maximum fluorescence emission rate of chlorophyll a extracts in ether is 30%, corresponding to a $k_{DF}$of 2, but this value probably does not represent in vivo k_{DF} of

chlorophyll in thylakoids. E. Pfündel, (1998) suggested a maximal PSII fluorescence quantum yield of PSII of 0.09, which would correspond to $k_{DF} = 10$. Tesa et al., (2018) found that at 75K, which made photochemical and nonphotochemical quenching impossible, the fluorescence quantum yield of an intact holly leaf was about 5%, resulting a k_{DF} of 19, a value used in Gu et al., (2019). But their measurements did not account for the self-absorption of fluorescence by leaf tissues and thus would lead to an overestimation of k_{DF}. If we assume 50% of the total fluorescence was measured in Tesa et al., (2018), corresponding to a self-absorptance of 0.5, a $k_{DF} = 10$ would also be obtained. The precise value of NPQ_7 is also uncertain. To estimate its magnitude, we accept, for the moment, the assumption of Kitajima & Butler, (1975) that PSI is an equal photochemical and non-photochemical quencher ($k_{PMI} = k_7$), the rate constant of non-photochemical quenching by $P700^+$), and further, $\Phi_{PSIm} = 0.98$ (Hogewoning et al., 2012; Nelson & Junge, 2015), then $NPQ_7 = 49$, according to Eq. S6. The actual value of NPQ_7 is likely less than 49 because recent studies have shown that $P700^+$ does not quench non-photochemically as efficiently as P700 does photochemically (Franck et al., 2002; Lazár, 2013; E. E. Pfündel et al., 2013; Schreiber & Klughammer, 2021; Trissl, 1997), which implies k_7 is less than k_{PMI}. k_D, k_F and therefore k_{DF} are assumed to be constant for both PSII and PSI.

It is difficult to measure s_{II} and s_I directly (even though might vary across species, canopy positions and physiological states) because PSII and PSI fluorescence emission overlap and because the foliar self-absorption depends on fluorescence wavelength. However, complexes of PSII and PSI can be isolated from leaves and their fluorescence emissions have been measured (Croce et al., 1996; Franck et al., 2002). Such measurements represent the best estimates for s_{II} and s_I so far.

SI – 5. Derivation of the balanced relationships between light and carbon reactions at the leaf level

To develop a strategy for modeling the regulatory light reaction variables (e.g., NPQ, q_{LII}) consistent with our empirical knowledge and theoretical understanding of photosynthesis, we consider the constraints set by the condition of balance between the light and carbon reactions, specifically by the requirement that the actual electron transport rate J_a estimated by the light reaction model equals that derived from the Farquhar-von Caemmerer-Berry (FvCB) biochemical model of photosynthesis (Farquhar et al., 1980). We use C_3 species and the lake model as an example. The balance relationships for C_4 species or the puddle model can be similarly derived.

Within the FvCB framework, the potential electron transport rate J_p is empirically calculated by BERNACCHI et al., (2003) at the leaf level:

$$J_p = \frac{\Phi_{PSIIm}\beta\alpha_{v\bar{i}s}PAR + J_{max} - \sqrt{(\Phi_{PSIIm}\beta\alpha_{v\bar{i}s}PAR + J_{max})^2 - 4\theta J_{max}\Phi_{PSIIm}\beta\alpha_{v\bar{i}s}PAR}}{2\theta} \quad \text{(S9)}$$

Here θ is an empirical curvature parameter and J_{max} is the maximum electron transport rate. The subscript p is used to differentiate the potential ETR of FvCB from the actual ETR J_a at the leaf level. $\alpha_{v\bar{i}s}$ is broadband absorption efficiency. Eq S9 is a root of the following quadratic equation:

$$\theta J_p^2 - (\Phi_{PSIIm}\beta\alpha_{v\bar{i}s}PAR + J_{max})J_p + J_{max}\Phi_{PSIIm}\beta\alpha_{v\bar{i}s}PAR = 0 \quad \text{(S10)}$$

which can be rewritten as:

$$\theta J_p^2 - J_{max}J_p - (J_p - J_{max})\Phi_{PSIIm}\beta\alpha_{v\bar{i}s}PAR = 0 \quad \text{(S11)}$$

Or equivalently,

$$J_p = \frac{J_{max} - J_p}{J_{max} - \theta J_p}\Phi_{PSIIm}\beta\alpha_{v\bar{i}s}PAR \quad \text{(S12)}$$

Eq S12 shows that the FvCB model for potential ETR is a recursive model as J_p occurs on both sides. It assumes the photochemical quantum yield of PSII is a function of ETR.

When the carboxylation is limited by RuBP regeneration, J_p becomes J_a. Comparing Eq S12 with Eqs 16-17 in Gu et al., (2019), we see that

$$\Phi_{PSII} = \frac{\Phi_{PSIIm}}{\frac{1+NPQ}{q_{LII}}(1 - \Phi_{PSIIm}) + \Phi_{PSIIm}} = \frac{J_{max} - J_p}{J_{max} - \theta J_a}\Phi_{PSIIm} \quad \text{(S13)}$$

If defining $q_{LN} = \frac{q_{LII}}{1 + NPQ}$, we have:

$$q_{LN} = \frac{1}{1 + \frac{1-\theta}{1-\Phi_{PSIIm}}\frac{J_a}{J_{max}-J_a}} \quad \textbf{(S14)}$$

When Rubisco limits carboxylation, the carboxylation rate supported by the actual ETR equals the Rubisco-limited carboxylation rate. Therefore,

$$A_n + R_d = \frac{J_a C_c}{4C_c + 8\Gamma^*} = \frac{V_{cmax}C_c}{C_c + K_c(1 + \frac{O}{K_o})} \quad \text{(S15)}$$

Eq S15 omits the cyclic electron transport around PSI and the Mehler reaction (water-water cycle) (Yin et al., 2009). Thus,

$$J_a = \frac{4C_c + 8\Gamma^*}{C_c + K_c(1 + \frac{O}{K_o})}V_{cmax} \quad \text{(S16)}$$

Combining Eq 17 in Gu et al., (2019) and Eq S16, and solving for q_{LN}, we have:

$$q_{LN} = \frac{q_{LII}}{1 + NPQ} = \frac{1 - \Phi_{PSIIm}}{\Phi_{PSIIm}\left(f_R\frac{\beta\alpha_{v\bar{i}s}PAR}{4V_{cmax}} - 1\right)} \quad \textbf{(S17)}$$

Here f_R denotes

$$f_R = \frac{C_c + K_c(1 + \frac{O}{K_o})}{C_c + 2\Gamma^*} \quad \text{(S18)}$$

When TPU limits carboxylation,

$$\frac{J_p C_c}{4C_c + 8\Gamma^*} = \frac{3TPU \cdot C_c}{C_c - (1 + 3\alpha_T)\Gamma^*} \quad \text{(S19)}$$

Here TPU is the rate of triose phosphate utilization and α_T is the non-returned fraction of the glycolate carbon recycled in the photorespiratory cycle. Therefore,

$$J = \frac{4C_c + 8\Gamma^*}{C_c - (1 + 3\alpha_T)\Gamma^*} 3TPU \quad \text{(S20)}$$

Combining Eq 16 in Gu et al., (2019) and Eq S20 leads to:

$$q_{LN} = \frac{q_{LII}}{1 + NPQ} = \frac{1 - \Phi_{PSIImax}}{\Phi_{PSIImax}\left(f_T \frac{\beta \alpha_{v\bar{i}s} PAR}{3TPU} - 1\right)} \quad \textbf{(S21)}$$

Here f_T is given by

$$f_T = \frac{C_c - (1 + 3\alpha_T)\Gamma^*}{C_c + 2\Gamma^*} \quad \text{(S22)}$$

V_{cmax}, J_{max}, and TPU are classic FvCB model parameters and have played key roles in photosynthesis and carbon cycle modeling. Eqs S14, S17, S21 show that they are intimately linked to regulatory light reaction variables via q_{LII} and NPQ.

SI – 6. Derivation of the toy model for $F_{\uparrow}(\lambda_F)$: Eq 8

We start from Eq 2c in the main text, by invoking several assumptions, which are necessary to simplify Eq 2c. Note that simplification is necessary in this context, but we are vigilant to the underlying assumptions and overall validity of the corollary. First , we assume a single value of Φ_{FII} and Φ_{FI}, denoted as $\bar{\Phi}_{FII}$ and $\bar{\Phi}_{FI}$ respectively, can effectively represent a whole canopy under steady state (**A1**). This is because the vertical heterogeneity in their leaf-scale variations can be largely attenuated once aggregated to the canopy scale (Chang et al., 2021), due to the compensation effect between photochemical and non-photochemical quenching, i.e., q_{LII} and NPQ for PSII, as well as q_I and q_{LI} for PSI. Note that this assumption may not hold under non-steady state when photochemistry and non-photochemistry are decoupled, a property exploited in PAM fluorometry. We also assume $\bar{p}$ can effectively represent the mean photosynthetic pigment content of the canopy (**A2**). Moreover, we assume that β and σ are relatively stable vertically, and can be effectively represented as a canopy-mean value, denoted as $\bar{\beta}$ and $\bar{\sigma}$ respectively (**A3**). No doubt these assumptions and simplifications can cause uncertainty but the alternative, which is to model vertical variations of these variables, can be equally or more uncertain, and will make any attempt to infer ecosystem structure and function from the observed $F_{\uparrow}(\lambda_F)$ exceedingly difficult. Further, we omit the small error that may be caused by a possible fluorescence wavelength λ_F shorter than the upper wavelength of the excitation irradiance (*e.g.*, around the O_2B band) and use $PAR(L) = \int_{400}^{700} I(L, \lambda_I) d\lambda_I$ (**A4**). Accepting these assumptions, Eq 3 in the main text becomes:

$$F_{\uparrow}(\lambda_F) = [\bar{\Phi}_{FII} s_{II}(\lambda_F)\bar{\beta} + \bar{\Phi}_{FI} s_I(\lambda_F)(1-\bar{\beta})]\bar{\sigma}\bar{p} \int_0^{LAI} [\varepsilon_{\uparrow}(L,\lambda_F) + \varepsilon_{\uparrow}(LAI,\lambda_F) r_s(\lambda_F) \varepsilon_{\downarrow}(L,\lambda_F)] PAR(L) dL \quad \text{(S23)}$$

To derive an analytical solution of the leaf-to-canopy integration, i.e., the integral of LAI, we here employ Beer's law to describe the attenuation of Chl*a*F emission and PAR inside a canopy:

$$\begin{cases} \varepsilon_{\uparrow}(L,\lambda_F) = \varepsilon_{\uparrow 0}(\lambda_F) e^{-k_{\lambda_F} L} & \text{(a)} \\ \varepsilon_{\downarrow}(L,\lambda_F) = \varepsilon_{\downarrow 0}(\lambda_F) e^{-k_{\lambda_F}(LAI-L)} & \text{(b)} \\ PAR(L) = PAR_0 e^{-k_{PAR} L} & \text{(c)} \end{cases} \quad \text{(S24)}$$

Here $\varepsilon_{\uparrow 0}$ and $\varepsilon_{\downarrow 0}$ denote the upward/downward escape probability of Chl*a*F emission for an infinitesimally thin leaf layer at TOC/BOC respectively; PAR_0 denotes incident light intensity at TOC; k_{λ_F} and k_{PAR} denote the extinction coefficients of Chl*a*F emission and PAR under Beer's law, respectively. Inserting Eqs S24 to S23 lead to Eq 8 in the main text (also shown below for clarify):

$$F_{\uparrow}(\lambda_F) = \underbrace{\varepsilon_{\uparrow 0}(\lambda_F) \left\{ \frac{1 - e^{-(k_{PAR}+k_{\lambda_F})LAI}}{(k_{PAR}+k_{\lambda_F})LAI} + \frac{\varepsilon_{\downarrow 0}(\lambda_F) r_s(\lambda_F) \left[e^{-2k_{\lambda_F} LAI} - e^{-(k_{PAR}+k_{\lambda_F})LAI} \right]}{(k_{PAR}-k_{\lambda_F})LAI} \right\}}_{\text{Structure}} \times \underbrace{[\bar{\Phi}_{FII} s_{II}(\lambda_F)\bar{\beta} + \bar{\Phi}_{FI} s_I(\lambda_F)(1-\bar{\beta})]}_{\text{Mean ChlaF yield}} \times \underbrace{\overbrace{\bar{p}LAI}^{\text{Pigment}} \times \bar{\sigma} PAR_0}_{\text{Light harvesting}} \quad \text{(8)}$$

We note that Eq 8 can be applied to a leaf by setting $LAI = 1$ and $r_s = 0$. At the leaf level, the light transmittance τ is related to light extinction coefficient at the leaf level, i.e., by $\tau = e^{-k}$; thus $\tau_{\lambda_F} = e^{-k_{\lambda_F}}$ and $\tau_{PAR} = e^{-k_{PAR}}$. The corresponding $F_{\uparrow}(\lambda_F)$ is then given by:

$$F_{\uparrow}(\lambda_F) = \underbrace{\varepsilon_{\uparrow 0} \frac{\tau_{\lambda_F}\tau_{PAR} - 1}{\ln(\tau_{\lambda_F}\tau_{PAR})}}_{\text{Structure}} \times \underbrace{[\bar{\Phi}_{FII} s_{II}(\lambda_F)\bar{\beta} + \bar{\Phi}_{FI} s_I(\lambda_F)(1-\bar{\beta})]}_{\text{Mean F yield}} \times \underbrace{\overbrace{\bar{p}}^{\text{Pigment}} \times \bar{\sigma} PAR}_{\text{Light harvesting}} \quad \text{(S25)}$$

SI – 7. Derivation of the redox state-based models to infer the actual canopy ETR from $F_{\uparrow}(\lambda_F)$: Eq 9

The relevance of SIF for monitoring photosynthesis rests on the fact that Chl*a*F emission is directly coupled to the linear ETR from PSII to PSI (Gu et al., 2019). This refers to the actual

ETR (denoted as J_a at the leaf level) instead of the potential ETR (i.e., J_p at the leaf level) in the commonly used FvCB model. As photochemistry, non-photochemical heat dissipation, and Chl*a*F emission form a closed system according to the principle of energy conservation, the relationship between the canopy-level actual ETR J_{aT} and $F_{\uparrow}(\lambda_F)$ can be expressed in terms of either redox states of PSII (i.e.., q_{LII}) or NPQ. For simplicity, we assume the contribution of soil reflected SIF is negligible (i.e., $r_s = 0$, **A5**).

We first extend the q_{LII}-based J_a equation at the leaf level derived in Gu et al., (2019; Eq 21 therein) to the canopy level (denoted as J_{aT}), leading to Eq 6 in the main text (also copied below for clarity):

$$J_{aT} = \int_0^{LAI} J_a(L)dL$$
$$= \frac{\Phi_{PSIIm}(1+k_{DF})}{1-\Phi_{PSIIm}} \int_0^{LAI} p(L)q_{LII}(L) \int_{\lambda_{Fmin}}^{\lambda_{Fmax}} \int_{\lambda_{Imin}}^{\lambda_F} \Phi_{FII}(L)s_{II}(\lambda_F)\beta(L,\lambda_I)\sigma(L,\lambda_I)I(L,\lambda_I)d\lambda_I d\lambda_F dL \quad (6)$$

Next we invoke **A4** as in the derivation of Eq 8 (SI-6 above), which leads to:

$$J_{aT}$$
$$= \int_0^{LAI} J_a(L)dL$$
$$= \int_0^{LAI} q_{LII}(L)\frac{\Phi_{PSIIm}(1+k_{DF})}{1-\Phi_{PSIIm}}\Phi_{FII}(L)\beta(L)p(L)\sigma(L)PAR(L)dL \quad (S26)$$

Further we invoke assumptions **A1-3** defined above. Moreover, we use the following function to capture the first order variation of q_{LII} with PAR within a canopy (Han et al., 2022):

$$q_{LII}(L) = a[PAR(L)]^b = aPAR_0^b e^{-bk_{PAR}L} = q_{LII0}e^{-bk_{PAR}L} \quad (S27)$$

Here, a and b are two empirical coefficients, and Eq S27 is used to describe the light attenuation with L. q_{LII0} is the fraction of open PSII reaction centers of a leaf at TOC. We insert Eqs S27 and S24c into Eq S26. After integration, we obtain

$$J_{aT} = \frac{aPAR_0^{b+1}\bar{p}\bar{\sigma}\bar{\beta}\Phi_{PSIIm}(1+k_{DF})\left[1-e^{-(b+1)k_{PAR}LAI}\right]}{(1-\Phi_{PSIIm})(b+1)k_{PAR}}\bar{\Phi}_{FII} \quad (S28)$$

Next, we derive an estimate of Φ_{FII} from $F_{\uparrow}(\lambda_F)$, using Eq 8 in the main text. To do so, we assume the ratio of Φ_{FI} to Φ_{FII} (and also the ratio of $\bar{\Phi}_{FI}$ to $\bar{\Phi}_{FII}$) is a constant (**A6)**.

$$\frac{\bar{\Phi}_{FI}}{\bar{\Phi}_{FII}} = \zeta \tag{S29}$$

Applying this ratio to Eq 8 and solving for $\bar{\Phi}_{FII}$, we have

$$\bar{\Phi}_{FII} = \frac{F_{\uparrow}(\lambda_F)(k_{\lambda_F} + k_{PAR})}{PAR_0 \left[s_{II}(\lambda_F)\bar{\beta} + \zeta s_I(\lambda_F)(1-\bar{\beta})\right] \bar{p}\bar{\sigma}\varepsilon_{\uparrow 0} \left\{1 - e^{-[k_{\lambda_F}+k_{PAR}]LAI}\right\}} \tag{S30}$$

Combining Eqs S28 and S30, we obtain the following q_L-based relationship between J_{aT} and $F_{\uparrow}(\lambda_F)$, i.e., Eq 9 in the main text (also included below for clarity).

$$J_{aT} = \underbrace{\frac{\left(\frac{k_{\lambda_F}}{k_{PAR}} + 1\right)\left[1 - e^{-(b+1)k_{PAR}LAI}\right]}{\varepsilon_{\uparrow 0}(\lambda_F)\left[1 - e^{-(k_{\lambda_F}+k_{PAR})LAI}\right]}}_{\text{Structure}} \times \underbrace{\frac{\Phi_{PSIIm}(1+k_{DF})}{1-\Phi_{PSIIm}}}_{\text{Constant}} \times \underbrace{\frac{\overbrace{\frac{aPAR_0^b}{b+1}}^{\text{Redox state}}}{s_{II}(\lambda_F) + \zeta s_I(\lambda_F)\frac{1-\bar{\beta}}{\bar{\beta}}}}_{\text{ChlaF weighting factor}} \times F_{\uparrow}(\lambda_F)$$

Note that in Eq 9, the physiology is represented by the redox state term of PSII of the canopy, which is collectively expressed as a function of the fraction of open PSII reaction centers of a leaf at the canopy top ($aPAR_0^b$).

SI – 8. Derivation of the redox state-based models to infer canopy-level GPP from $F_{\uparrow}(\lambda_F)$: Eq 10

At the leaf level, once J_a is known, photosynthesis can be calculated by assuming all electrons from PSII are consumed either in carboxylation (CO_2 assimilation) or oxygenation (photorespiration) and no other electron sinks exist and the light-carbon reactions are in perfect balance (**A7**). This assumption is fairly accurate in normal conditions but may be violated when plants are under stress (Tcherkez & Limami, 2019). To calculate photosynthesis, one must further decide whether the carboxylation is limited by the supply of reducing power NADPH or energy currency ATP. In typical applications of the FvCB model, NADPH is assumed to be limiting (**A8**). These assumptions are adopted here to calculate photosynthesis of the canopy denoted as GPP_T, and hence leads to Eq 7 in the main text (also copied below for clarity).

$$GPP_T \begin{cases} = \int_0^{LAI} \frac{C_c(L)-\Gamma^*(L)}{4C_c(L)+8\Gamma^*(L)} J_a(L)dL \\ = \frac{\Phi_{PSIIm}(1+k_{DF})}{1-\Phi_{PSIIm}} \int_0^{LAI} \frac{C_c(L)-\Gamma^*(L)}{4C_c(L)+8\Gamma^*(L)} q_{LII}(L) \int_{\lambda_{Fmin}}^{\lambda_{Fmax}} \int_{\lambda_{Imin}}^{\lambda_F} \Phi_{FII}(L) s_{II}(\lambda_F)\beta(L,\lambda_I)\sigma(L,\lambda_I)I(L,\lambda_I)d\lambda_I d\lambda_F dL & \text{(C3) (a)} \\ = \int_0^{LAI} \frac{1-x}{3} J_a(L)dL \\ = \frac{\Phi_{PSIIm}(1+k_{DF})}{1-\Phi_{PSIIm}} \frac{1-x}{3} \int_0^{LAI} q_{LII}(L) \int_{\lambda_{Fmin}}^{\lambda_{Fmax}} \int_{\lambda_{Imin}}^{\lambda_F} \Phi_{FII}(L) s_{II}(\lambda_F)\beta(L,\lambda_I)\sigma(L,\lambda_I)I(L,\lambda_I)d\lambda_I d\lambda_F dL & \text{(C4) (b)} \end{cases} \tag{7}$$

Here C_c is the CO_2 partial pressure in the stroma of chloroplast and Γ^* is the CO_2 compensation point in the absence of day respiration. We further assume that the electron (e^-) use efficiency of carboxylation, $\frac{C_c - \Gamma^*}{4C_c + 8\Gamma^*}$ does not vary along the depth of a canopy, which requires either C_c and Γ^* are uniform vertically or C_c is much larger than Γ^* (**A9**). Assuming **A1-A9** and inserting Eqs S24 and 27 into Eq 7, we have the q_{LII}-based GPP-$F_\uparrow(\lambda_F)$ relationship, Eq 10 in the main text (also included below for completeness):

$$GPP_T = \underbrace{\frac{\left(\frac{k_{\lambda_F}}{k_{PAR}} + 1\right)\left[1 - e^{-(b+1)k_{PAR}LAI}\right]}{\varepsilon_{\uparrow 0}(\lambda_F)\left[1 - e^{-(k_{\lambda_F} + k_{PAR})LAI}\right]}}_{\text{Structure}} \times \underbrace{\frac{\Phi_{PSIIm}(1 + k_{DF})}{1 - \Phi_{PSIIm}}}_{\text{Constant}} \times \underbrace{\frac{\overbrace{\frac{aPAR_0^b}{b+1}}^{\text{Redox state}}}{s_{II}(\lambda_F) + \zeta s_I(\lambda_F)\frac{1-\bar{\beta}}{\bar{\beta}}}}_{\text{ChlaF weighting factor}} \times F_\uparrow(\lambda_F)$$

$$\times \begin{cases} \frac{C_c - \Gamma^*}{4C_c + 8\Gamma^*} & \text{(C3) (a)} \\ \frac{1-x}{3} & \text{(C4) (b)} \end{cases}$$

Reference

Baker, N. R. (2008). Chlorophyll Fluorescence: A Probe of Photosynthesis In Vivo. Annual Review of Plant Biology, 59(1), 89–113. https://doi.org/10.1146/annurev.arplant.59.032607.092759

Ballottari, M., Alcocer, M. J. P., D'Andrea, C., Viola, D., Ahn, T. K., Petrozza, A., Polli, D., Fleming, G. R., Cerullo, G., & Bassi, R. (2014). Regulation of photosystem I light harvesting by zeaxanthin. Proceedings of the National Academy of Sciences, 111(23). https://doi.org/10.1073/pnas.1404377111

BERNACCHI, C. J., PIMENTEL, C., & LONG, S. P. (2003). In vivo temperature response functions of parameters required to model RuBP-limited photosynthesis. Plant, Cell & Environment, 26(9), 1419–1430. https://doi.org/10.1046/j.0016-8025.2003.01050.x

Björkman, O., & Demmig, B. (1987). Photon yield of O2 evolution and chlorophyll fluorescence characteristics at 77 K among vascular plants of diverse origins. Planta. https://doi.org/10.1007/BF00402983

Bukhov, N. G., & Carpentier, R. (2003). Measurement of photochemical quenching of absorbed quanta in photosystem I of intact leaves using simultaneous measurements of absorbance changes at 830 nm and thermal dissipation. Planta, 216(4), 630–638. https://doi.org/10.1007/s00425-002-0886-2

Caffarri, S., Tibiletti, T., Jennings, R., & Santabarbara, S. (2014). A comparison between plant photosystem I and photosystem II architecture and functioning. Current Protein & Peptide Science, 15(4), 296–331. https://doi.org/10.2174/1389203715666140327102218

Chang, C. Y., Wen, J., Han, J., Kira, O., LeVonne, J., Melkonian, J., Riha, S. J., Skovira, J., Ng, S., Gu, L., Wood, J. D., Näthe, P., & Sun, Y. (2021). Unpacking the drivers of diurnal dynamics of sun-induced chlorophyll fluorescence (SIF): Canopy structure, plant physiology, instrument configuration and retrieval methods. Remote Sensing of Environment, 265, 112672. https://doi.org/10.1016/j.rse.2021.112672

Croce, R., Zucchelli, G., Garlaschi, F. M., Bassi, R., & Jennings, R. C. (1996). Excited State Equilibration in the Photosystem I−Light-Harvesting I Complex: P700 Is Almost Isoenergetic with Its Antenna. Biochemistry, 35(26), 8572–8579. https://doi.org/10.1021/bi960214m

Farquhar, G. D., Caemmerer, S., & Berry, J. A. (1980). A biochemical model of photosynthetic CO2 assimilation in leaves of C3 species. Planta, 149(1), 78-90–90.

Franck, F., Juneau, P., & Popovic, R. (2002). Resolution of the Photosystem I and Photosystem II contributions to chlorophyll fluorescence of intact leaves at room temperature. Biochimica et Biophysica Acta - Bioenergetics, 1556(2–3), 239–246. https://doi.org/10.1016/S0005-2728(02)00366-3

Gu, L., Han, J., Wood, J. D., Chang, C. Y. Y., & Sun, Y. (2019). Sun-induced Chl fluorescence and its importance for biophysical modeling of photosynthesis based on light reactions. New Phytologist, 223(3), 1179–1191. https://doi.org/10.1111/nph.15796

Han, J., Chang, C. Y. Y., Gu, L., Zhang, Y., Meeker, E. W., Magney, T. S., Walker, A. P., Wen, J., Kira, O., McNaull, S., & Sun, Y. (2022). The physiological basis for estimating photosynthesis from Chla fluorescence. New Phytologist, 234(4), 1206–1219. https://doi.org/10.1111/NPH.18045

Hogewoning, S. W., Wientjes, E., Douwstra, P., Trouwborst, G., Ieperen, W. van, Croce, R., & Harbinson, J. (2012). Photosynthetic Quantum Yield Dynamics: From Photosystems to Leaves. The Plant Cell, 24(5), 1921–1935. https://doi.org/10.1105/tpc.112.097972

Jegerschoeld, C., Virgin, I., & Styring, S. (1990). Light-dependent degradation of the D1 protein in photosystem II is accelerated after inhibition of the water splitting reaction. Biochemistry, 29(26), 6179–6186. https://doi.org/10.1021/bi00478a010

JOHNSON, G. N., YOUNG, A. J., SCHOLES, J. D., & HORTON, P. (1993). The dissipation of excess excitation energy in British plant species. Plant, Cell and Environment, 16(6), 673–679. https://doi.org/10.1111/j.1365-3040.1993.tb00485.x

Kitajima, M., & Butler, W. L. (1975). Quenching of chlorophyll fluorescence and primary photochemistry in chloroplasts by dibromothymoquinone. Biochimica et Biophysica Acta (BBA) - Bioenergetics, 376(1), 105–115. https://doi.org/10.1016/0005-2728(75)90209-1

Lazár, D. (2013). Simulations show that a small part of variable chlorophyll a fluorescence originates in photosystem I and contributes to overall fluorescence rise. Journal of Theoretical Biology, 335, 249–264. https://doi.org/10.1016/j.jtbi.2013.06.028

Nelson, N. (2009). Plant Photosystem I – The Most Efficient Nano-Photochemical Machine. Journal of Nanoscience and Nanotechnology, 9(3), 1709–1713. https://doi.org/10.1166/jnn.2009.SI01

Nelson, N., & Junge, W. (2015). Structure and Energy Transfer in Photosystems of Oxygenic Photosynthesis. Annual Review of Biochemistry, 84(1), 659–683. https://doi.org/10.1146/annurev-biochem-092914-041942

Pfündel, E. (1998). Estimating the contribution of photosystem I to total leaf chlorophyll fluorescence. Photosynthesis Research, 56(2), 185–195. https://doi.org/10.1023/A:1006032804606

Pfündel, E. E., Klughammer, C., Meister, A., & Cerovic, Z. G. (2013). Deriving fluorometer-specific values of relative PSI fluorescence intensity from quenching of F 0 fluorescence in leaves of Arabidopsis thaliana and Zea mays. Photosynthesis Research, 114(3), 189–206. https://doi.org/10.1007/s11120-012-9788-8

Schreiber, U., & Klughammer, C. (2021). Evidence for variable chlorophyll fluorescence of photosystem I in vivo. Photosynthesis Research, 149(1–2), 213–231. https://doi.org/10.1007/s11120-020-00814-y

Sonoike, K. (2011). Photoinhibition of photosystem I. Physiologia Plantarum, 142(1), 56–64. https://doi.org/10.1111/j.1399-3054.2010.01437.x

Tcherkez, G., & Limami, A. M. (2019). Net photosynthetic CO2 assimilation: More than just CO2 and O2 reduction cycles. New Phytologist, 223(2), 520–529. https://doi.org/10.1111/NPH.15828

Tesa, M., Thomson, A., & Gakamsky, A. (2018). Temperature-dependent quantum yield of fluorescence from plant leaves. Application Notes in Edinburgh Instruments., AN_P41. https://www.edinst.com/wp-content/uploads/2018/04/Temperature-Dependent-Quantum-Yield-of-Fluorescence-from-Plant-Leaves.pdf

Tian, L., Xu, P., Chukhutsina, V. U., Holzwarth, A. R., & Croce, R. (2017). Zeaxanthin-dependent nonphotochemical quenching does not occur in photosystem I in the higher plant Arabidopsis thaliana. Proceedings of the National Academy of Sciences, 114(18), 4828–4832. https://doi.org/10.1073/pnas.1621051114

van der Tol, C. V. D., Berry, J. A., Campbell, P. K. E., & Rascher, U. (2014). Models of fluorescence and photosynthesis for interpreting measurements of solar-induced chlorophyll fluorescence. Journal of Geophysical Research: Biogeosciences. https://doi.org/10.1002/2014JG002713

Trissl, H.-W. (1997). Determination of the quenching efficiency of the oxidized primary donor of Photosystem I. Photosynthesis Research, 54(3), 237–240. https://doi.org/10.1023/A:1005981016835

Yin, X., Struik, P. C., Romero, P., Harbinson, J., Evers, J. B., Putten, P. E. L. V. D., & Vos, J. (2009). Using combined measurements of gas exchange and chlorophyll fluorescence to estimate parameters of a biochemical C 3 photosynthesis model: A critical appraisal and a new integrated approach applied to leaves in a wheat (Triticum aestivum) canopy. Plant, Cell & Environment, 32(5), 448–464. https://doi.org/10.1111/j.1365-3040.2009.01934.x